Multi-Antenna Spectrum Sensing with Alpha-Stable Noise for Cognitive Radio-Enabled IoT

Junlin Zhang, Mingqian Liu, *Member, IEEE*, Yunfei Chen, *Senior Member, IEEE*, Nan Zhao, *Senior Member, IEEE*, Yuting Han and Ning Zhang, *Senior Member, IEEE*

***Abstract*—Cognitive radio-enabled Internet of Things (CR-IoT) is considered as a promising technology to handle spectrum scarcity for IoT applications. Spectrum sensing enables unlicensed secondary users to exploit spectrum holes under the condition of avoiding interference with primary users in CR-IoT networks. Previous studies often assume that the noise is Gaussian while ignoring the influence of non-Gaussian noise. Moreover, multi-antenna-based spectrum sensing algorithms only consider the partial information of covariance matrix. This paper develops two multi-antenna-based spectrum sensing schemes, using fractional low-order covariance matrices to address the issue of performance degradation in impulsive noise. Specifically, the first scheme, namely, diagonal element weighting detection, exploits the diagonal element weighting of the fractional low-order covariance matrix. The latter scheme is called off-diagonal element weighting detection, which adopts the diagonal matrix weighting strategy that exploits the off-diagonal elements of fractional low-order covariance matrices. The approximate analytical expressions of the false alarm probability and detection probability are derived. These developed schemes do not employ any priori knowledge of the primary user signal. Simulation results indicate that two proposed schemes achieve acceptable performance and are robust to the characteristic exponent of the alpha-stable noise, e.g., these proposed methods could achieve a detection probability of 90% with a false alarm probability of 0.1 at GSNR = -16dB, respectively.**

***Index Terms*—Cognitive radio-enabled Internet of Things (CR-IoT), fractional low-order covariance matrix, multiple antennas, spectrum sensing, symmetric alpha-stable distribution.**

I. Introduction

INTERNET of Things (IoT) can provide large-scale connectivity for smart devices and information sensors to achieve intelligent identification, positioning, tracking, monitoring, etc [1]. It is widely applied in environmental protection, public safety, industrial monitoring, personal health, urban air transportation, etc [2], [3]. This quick development leads to spectrum scarcity due to serious spectrum congestion in IoT traffic. Hence, cognitive radio (CR) has been introduced to develop CR-enabled IoT (CR-IoT) networks [4]. The CR-IoT network is a novel paradigm of self-organized and distributed networks, which provides a possible approach for the sensor node to use the limited scarce spectrum resources efficiently [5], [6]. In the CR-IoT network, a massive number of sensor nodes are equipped to perform cognitive tasks in complex communication scenarios. Generally, CR-IoT frame can be divided into two processes, namely spectrum sensing and data transmission [7]. Spectrum sensing aims to detect the spectrum state of IoT devices, i.e., idle or busy, thus avoiding interfering with primary IoT-devices when cognitive IoT-devices transmit data. Accordingly, the convenient and efficient spectrum sensing scheme should be carefully considered to adopt a dynamic spectrum access mechanism for effectively improving spectrum utilization in CR-IoT networks [8], [9].

Most existing sensing methods assume Gaussian noise [10]–[16]. In particular, multi-antenna-based spectrum sensing algorithms can improve performance by taking advantage of spatial degree of freedom. For example, a multi-antenna iterative detection method was proposed using the SUMPLE combining concept in [17]. However, this algorithm suffers from noise uncertainty. In [18], Gaussian noise model was established and a maximum-to-minimum eigenvalue-based algorithm was proposed, which adopts the ratio of the maximum eigenvalue to the minimum eigenvalue as the detection statistic. In [19], a detection statistic was constructed based on the maximum local variance and average local variance to determine whether the spectrum is free. The above two methods overcome the noise uncertainty at the cost of high computational complexity. Reference [20] developed two schemes based on the generalized likelihood ratio test under interference. These two schemes provide good performance using the knowledge of interference's statistical characteristics, but again with high computational complexity. Chen *et al*. applied the real-valued weights for the covariance matrix to create a covariance-based detector in [21]. This detector reduces computational complexity. In [22], a cyclostationary-based detector was presented with multiple antennas, which exploits the eigenvalues of the cyclic covariance matrix of primary signals. However, the cyclostationary analysis involved in this detector requires complex computations. The simple F-test-based detector based

This work was supported by the National Natural Science Foundation of China under Grant 62301380, 62231027 and 62071364, in part by the Natural Science Basic Research Program of Shaanxi under Grant 2024JC-JCQN-63, in part by the China Postdoctoral Science Foundation under Grant 2022M722504, in part by the Postdoctoral Science Foundation of Shaanxi Province under Grant 2023BSHEDZZ169, in part by the Key Research and Development Program of Shaanxi under Grant 2023-YBGY-249, in part by the Guangxi Key Research and Development Program under Grant 2022AB46002 and in part by the Fundamental Research Funds for the Central Universities under Grant XJSJ23090. *(Corresponding author: Mingqian Liu.)*

J. Zhang, M. Liu and Y. Han are with the State Key Laboratory of Integrated Service Networks, Xidian University, Shaanxi, Xi'an 710071, China (e-mail: zhangjunlin@xidian.edu.cn; mqliu@mail.xidian.edu.cn; hytxidian@163.com).

Y. Chen is with Department of Engineering, University of Durham, Durham, UK DH1 3LE (e-mail: Yunfei.Chen@durham.ac.uk).

N. Zhao is with the School of Information and Communication Engineering, Dalian University of Technology, Dalian 116024, China (e-mail: zhaonan@dlut.edu.cn).

N. Zhang is with the Department of Electrical and Computer Engineering, University of Windsor, Windsor, ON N9B 3P4, Canada (e-mail: ning.zhang@uwindsor.ca).

on singular value decomposition was presented for multi-antenna CR in [23]. The detector can perform well without requiring prior knowledge of the channel state information. In [24], Chae *et al*. introduced the convolutional neural network (CNN) to design a deep-spectrum sensing model. But the performance of the deep learning-based detector relies heavily on the training examples.

The above existing methods have good detection performance in Gaussian noise, but signals may be corrupted by non-Gaussian noise or interference under complex circumstances, such as man-made pulses, voice signals, low-frequency atmospheric noise, microwave appliances, mutual interference between users, out-of-band leakage, interference from ultra-bandwidth systems, etc [25]. Therefore, spectrum sensing needs to consider the influence of non-Gaussian noise. Impulsive noise often has strong impulsiveness and the tail is more serious than Gaussian noise [26]. In particular, the alpha-stable distribution is a suitable model to describe this type of impulsive noise [27].

To address spectrum sensing in alpha-stable noise, several works have been investigated in [28]–[36]. The algorithm presented in [28] utilized the bi-parameter CGM model to describe the alpha-stable noise and exploited the maximin approach. Since the traditional spectrum sensing method based on the second-order statistics is not suitable for non-Gaussian noise, a spectrum sensing scheme using fractional low-order moments was proposed in [29]. Shabani *et al*. in [30] proposed an enhanced energy detector based on the order statistics. The above two methods improve energy detection, which is sensitive to noise uncertainty. In [31], two new multi-antenna-based spectrum sensing methods were proposed for the symmetric α-stable ($S\alpha S$) noise. The first method used the covariation of $S\alpha S$ noise. The second method filtered the corrupted signal before applying the traditional spectrum sensing method. However, these two sensing methods need to determine the detection thresholds experimentally, limiting their application of the spectrum sensing algorithm. In [32], a novel goodness-of-fit test was developed based on the geometric power. This method has a high probability of detection in alpha-stable noise. To improve the performance, Liu *et al*. employed the generalized maximum correntropy to formulate the cooperative spectrum sensing cost function under $S\alpha S$ noise in [33]. A robust spectrum sensing scheme was proposed based on the hyperbolic tangent function in [34], [35] for non-Gaussian noise. The proposed scheme achieves a considerable performance gain but is computationally expensive. References [36] developed a CNN detector for $S\alpha S$ noise by exploiting one-dimensional input composed of the original signals. The proposed detector achieves satisfactory performance, also has high computational complexity.

Despite the improved detection performance of the above methods in the presence of heavy-tailed noise, multi-antenna-based sensing schemes do not fully taking advantages of the excellence of spatial degree of freedom. Moreover, covariance-based methods only consider partial information of covariance matrix, which does not fully utilize all the elements to optimize the detection statistics. In this paper, we first introduce the fractional low-order covariance matrix (FLOCM) of the received signal by using multiple antennas. Then, two novel detection statistics are extracted from the weighted FLOCM, which utilize the diagonal elements and off-diagonal elements. Finally, spectrum sensing is conducted by comparing two detection statistics with the corresponding detection thresholds. The contributions of this work are summarized as follows.

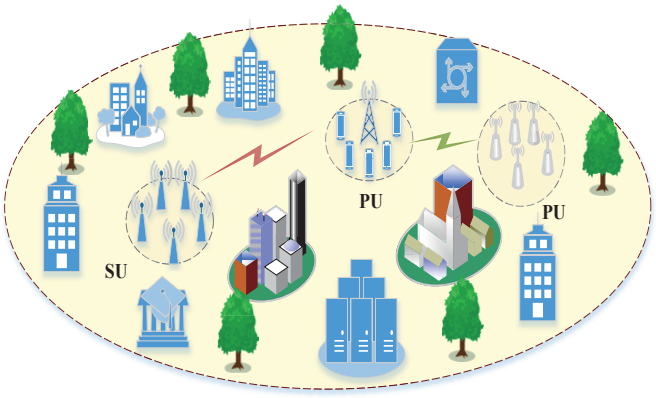

Fig. 1. Scenario of spectrum sensing in CR-IoT networks

- The CR-IoT networks may operate in practice under non-Gaussian noise, such as man-made impulsive noise. We study the spectrum sensing method under non-Gaussian noise to improve the spectrum utilization efficiency.
- Unlike existing works on spectrum sensing, we make full use of the fractional low-order covariance matrices to develop two novel multi-antennas-based sensing schemes for CR-IoT networks. These two schemes exploit the diagonal elements and off-diagonal elements in the fractional low-order covariance matrix to extract weighted detection statistics.
- We derive the approximate analytical expressions of the false alarm probability, detection probability and detection thresholds for the two proposed detection schemes in the presence of $S\alpha S$ noise.

The rest of this paper is organized as follows. In Section II, the system model is described in detail. In Section III, the spectrum sensing scheme based on the fractional low-order covariance matrix is introduced. The spectrum sensing performance is analyzed in Section IV. Simulation results are given in Section V. Finally, conclusions are drawn in Section VI.

II. System Model

A. System Model

Consider a CR-IoT network as shown in Fig. 1, which has a single primary user and a single secondary user equipped with M-element antenna. It is assumed that the PU transmitter works continuously during the spectrum sensing. In the considered scenario, spectrum sensing determines the state of spectrum use by detecting the presence of the PU signal, which can be regarded as the binary hypothesis testing problem. At the sampling time k, the two hypotheses can be expressed as

$$\begin{aligned} \mathcal{H}_0 &: \mathbf{x}(k) = \mathbf{w}(k), && \text{if PU is absent,} \\ \mathcal{H}_1 &: \mathbf{x}(k) = \mathbf{h}s(k) + \mathbf{w}(k), && \text{if PU is present,} \end{aligned} \tag{1}$$

where $\mathcal{H}_0$ indicates that the primary signal is absent, and $\mathcal{H}_1$ indicates that the PU is present, $\mathbf{x}(k) = [x_1(k), ..., x_m(k), ..., x_M(k)]^{\mathrm{T}}$ denotes the signal received by the SU, and $x_m(k)$ is the received signal at the sampling time k by the m-th antenna; $\mathbf{w}(k) = [w_1(k), ..., w_m(k), ..., w_M(k)]^{\mathrm{T}}$ is the additive noise, $s(k)$ is the signal transmitted by the PU, and $s(k)$ is the transmitted signal at the k-th time. $\mathbf{h} = [h_1, ..., h_m, ..., h_M]^T$, h_m is the channel gain of the m-th receiving antenna. The additive noise vector $\mathbf{w}(k)$ follows the $S\alpha S$ distribution with each elements is an independent identical distribution (IID) with a characteristic exponent α and a dispersion coefficient γ. The PU signal $s(k)$ is independent of the noise.

B. Noise Model

Note that the probability density function (PDF) of the alpha-stable random variable has no closed form. It is usually expressed by the following characteristic function

$$\varphi(t) = \exp\{j\delta t - \gamma|t|^{\alpha}[1 + j\beta \mathrm{sgn}(t) w(t,\alpha)]\}, \quad (2)$$

where $\mathrm{sgn}(t) = \begin{cases} 1, t > 0 \\ 0, t = 0 \\ -1, t < 0 \end{cases}$ is the sign function, $w(t,\alpha) = \begin{cases} \tan(\frac{\alpha\pi}{2}), \alpha \neq 1 \\ \frac{2}{\pi}\log|t|, \alpha = 1 \end{cases}$, α is the characteristic exponent that determines the impulsiveness of the stable distribution and the tailing of its PDF, and its value range is $0 < \alpha \leq 2$. The smaller α, the more impulsive noise is, and the larger the tailing. When $\alpha = 2$, it become a Gaussian distribution, whose variance is 2γ. It can be seen that the Gaussian distribution is only a special case of alpha-stable distribution. γ is the dispersion coefficient, and $\gamma \geq 0$. β is a symmetric parameter, which determines the symmetric characteristics of the distribution, and its value range is $-1 \leq \beta \leq 1$. δ is a displacement parameter representing the position of the PDF of the alpha-stable distribution. In this paper, the standard $S\alpha S$ distribution is used, i.e., $\beta = 0$, $\delta = 0$, and $\gamma = 1$.

The $S\alpha S$ noise have infinite variance. Therefore, based on the dispersion coefficient γ of the alpha-stable distribution and the variance σ_s^2 of the signal, the generalized signal-to-noise ratio (GSNR) is used as [20]

$$\mathrm{GSNR} = 10\log_{10}\left(\frac{\sigma_{\mathrm{s}}^2}{\gamma}\right). \quad (3)$$

III. Spectrum Sensing Using Fractional Low Order Covariance Matrix

A. Spectrum Sensing Using the Diagonal Element Weighting

Traditional spectrum sensing algorithms perform well with Gaussian noise. However, in most practical CR applications, the ambient noise exhibits significant non Gaussian impulsiveness. As a result, previous spectrum sensing algorithms may degrade or even fail. To overcome these shortcomings, two novel detection schemes based on the FLOCM are proposed in this section.

The statistical FLOCM of the received signal is given by

$$\mathbf{G}_{\mathbf{x}} = \mathbb{E}\left\{|\mathbf{x}(k)|^{b/2}\left(|\mathbf{x}(k)|^{b/2}\right)^{\mathrm{H}}\right\}. \quad (4)$$

where $\mathbb{E}\{\cdot\}$ denotes the statistical expectation, $[\cdot]^H$ represents the conjugate transpose, $|\cdot|$ represents absolute value. $|\mathbf{x}(k)|^{b/2} = [|x_1(k)|^{b/2}, \cdots, |x_m(k)|^{b/2}, \cdots, |x_M(k)|^{b/2}]^{\mathrm{T}}$. The matrix $\mathbf{G}_{\mathbf{x}}$ performs low-order moment ($0 < b < \alpha$) operations on the received signal $\mathbf{x}(k)$ to solve the problem that the alpha-stable distribution does not exhibit finite second-order moment. Meanwhile, the non-linear operation employed by FLOCM helps to reduce the impulsiveness of the noise so as to improve spectrum sensing performance. Note that the preferred value of b can be further optimized.

Considering that it is difficult to obtain the statistical FLOCM $\mathbf{G}_{\mathbf{x}}$ of the received signal $\mathbf{x}(k)$ in most practical applications, and the sample fraction low-order covariance matrix (SFLOCM) $\hat{\mathbf{G}}_{\mathbf{x}}$ is used to approximate $\mathbf{G}_{\mathbf{x}}$ as

$$\begin{aligned}\hat{\mathbf{G}}_{\mathbf{x}} &= \frac{1}{K}\sum_{k=1}^{K}|\mathbf{x}(k)|^{b/2}\left(|\mathbf{x}(k)|^{b/2}\right)^{\mathrm{H}} \\ &= \begin{bmatrix} \hat{g}_{11} & \cdots & \hat{g}_{1M} \\ & \ddots & \\ \vdots & \hat{g}_{mm} & \vdots \\ & & \ddots \\ \hat{g}_{M1} & \cdots & \hat{g}_{MM} \end{bmatrix}, \end{aligned} \quad (5)$$

where $|\mathbf{x}(k)|^{b/2} = \left[|x_1(k)|^{b/2}, |x_2(k)|^{b/2}, \cdots, |x_M(k)|^{b/2}\right]^{\mathrm{T}}$, b represents a fractional order. In $\hat{\mathbf{G}}_{\mathbf{x}}$, the diagonal elements can be calculated as $\hat{g}_{mm} = \frac{1}{K}\sum_{k=1}^{K}|x_m(k)|^{b/2}|x_m^*(k)|^{b/2}$, and the off-diagonal elements can be calculated as $\hat{g}_{mn} = \frac{1}{K}\sum_{k=1}^{K}|x_m(k)|^{b/2}|x_n^*(k)|^{b/2}$.

Since the PU signal is usually modulated, the correlation of the signal samples is significantly higher than that of the additive noise. For a fading channel with alpha-stable noise, when $\mathcal{H}_0$ is ture, the difference between the diagonal elements in the SFLOCM $\hat{\mathbf{G}}_{\mathbf{x}}$ is minimal. This is because there is no signal transmission from the PU, and the value of the diagonal elements is only dependent of the noise. If $\mathcal{H}_1$ holds, the difference of the diagonal elements in the SFLOCM $\hat{\mathbf{G}}_{\mathbf{x}}$ due to PU signal, and the value of the diagonal elements becomes larger. Hence, the diagonal elements of the SFLOCM $\hat{\mathbf{G}}_{\mathbf{x}}$ exhibit significant differences betweeen $\mathcal{H}_0$ and $\mathcal{H}_1$.Using these properties, the diagonal elements in the SFLOCM $\hat{\mathbf{G}}_{\mathbf{x}}$ can be employed to weight the matrix $\hat{\mathbf{G}}_{\mathbf{x}}$ so as to improve spectrum detection performance. Consequently, the detection statistic is constructed using the weighted SFLOCM $\hat{\mathbf{G}}_{\mathbf{x}}$ as

$$\mathcal{T}_1 = \sum_{m=1}^{M}\sum_{n\neq m}^{M}\frac{\hat{g}_{nn} - \mu_{10}}{\sigma_{10}}\hat{g}_{mm} \underset{\mathcal{H}_1}{\overset{\mathcal{H}_0}{\lessgtr}} \psi_1, \quad (6)$$

where μ_{10} and σ_{10} respectively represent the mean and standard variance of the diagonal elements in the SFLOCM $\hat{\mathbf{G}}_{\mathbf{x}}$ under $\mathcal{H}_0$, i.e., $\mu_{10} = \mathbb{E}\{\hat{g}_{mm}|\mathcal{H}_0\}$ and $\sigma_{10} = \sqrt{\mathbb{D}\{\hat{g}_{mm}|\mathcal{H}_0\}}$. The normalization of the diagonal elements as weights facilitates the derivation of the detection threshold ψ_1. If $\mathcal{T}_1 \geq \psi_1$, the primary signal is detected by the SU, and the licensed spectrum is occupied by PU; otherwise, the

Algorithm 1 Spectrum sensing based on the SFLOCM using the diagonal element weighting

1: Initialize parameters b, α, γ;
2: Construct the SFLOCM $\hat{\mathbf{G}}_{\mathbf{x}}$;
3: Calculate the mean μ_{10} and standard variance σ_{10} of the diagonal elements in the SFLOCM $\hat{\mathbf{G}}_{\mathbf{x}}$ and the detection statistics $\mathcal{T}_1$;
4: Determine the detection threshold ψ_1. See Section IV-A-1 for the derivation of this part.
5: Spectrum detection: If $\mathcal{T}_1 \geq \psi_1$, the PU signal exists; otherwise, the signal does not exist.

Algorithm 2 Spectrum sensing based on the SFLOCM using the off-diagonal element weighting

1: Initialization parameters b, α, γ;
2: Construct the SFLOCM $\hat{\mathbf{G}}_{\mathbf{x}}$;
3: Calculate the mean μ_{20} and standard variance σ_{20} of the diagonal elements in the SFLOCM and the detection statistics $\mathcal{T}_2$;
4: Determine the detection threshold ψ_2. See Section IV-B-1 for the derivation of this part.
5: Spectrum detection: If $\mathcal{T}_2 \geq \psi_2$, the PU signal exists; otherwise, the signal does not exist.

PU is absent, and the licensed spectrum is idle. The spectrum sensing scheme based on the SFLOCM using the diagonal element weighting (SFLOCM-DEW) has been summarized in Algorithm 1.

B. Spectrum Sensing Using the Off-diagonal Element Weighting

The above sensing scheme can well detect the presence of the PU signal. However, under $\mathcal{H}_0$, the off-diagonal elements in the SFLOCM are smaller than those under $\mathcal{H}_1$. Meanwhile, under the two hypotheses, the range of the off-diagonal elements is much larger than that of the diagonal elements. Therefore, the scheme proposed in Section III-A can be improved by using the off-diagonal element weighting (SFLOCM-ODEW). The SFLOCM-ODEW scheme takes the off-diagonal elements as weighting factors to weight the detection statistics. The proposed scheme makes full use of the characteristic that the value of the weighted diagonal element under $\mathcal{H}_1$ is much larger than that under $\mathcal{H}_0$. Under this framework, the detection statistics can be constructed as follows. First, the off-diagonal elements in the SFLOCM are normalized and summed. Then, it is weighted to the diagonal elements and summed to detect the presence or absence of the PU. Hence, the detection statistics can be expressed as

$$\mathcal{T}_2 = \sum_{m=1}^{M} \hat{g}_{mm} \sum_{\substack{p=1 \\ p\neq m}}^{M} \sum_{\substack{q=1 \\ q\neq p\neq m}}^{M} \frac{\hat{g}_{pq} - \mu_{20}}{\sigma_{20}} \underset{\mathcal{H}_1}{\overset{\mathcal{H}_0}{\lessgtr}} \psi_2, \tag{7}$$

where μ_{20} and σ_{20} represent the mean and standard variance of the off-diagonal elements in the SFLOCM under $\mathcal{H}_0$, i.e., $\mu_{20} = \mathbb{E}\{\hat{g}_{pq}|\mathcal{H}_0\}$ and $\mu_{20} = \mathbb{E}\{\hat{g}_{pq}|\mathcal{H}_0\}$, ψ_2 is the detection threshold. The spectrum sensing scheme based on the SFLOCM using the off-diagonal element weighting (SFLOCM-ODEW) has been summarized in Algorithm 2.

IV. Spectrum Sensing Performance Analysis

In this section, we will derive the analytical expressions of the false alarm probability, detection probability, and detection threshold.

A. Performance of SFLOCM-DEW Scheme

1) False alarm probability and detection threshold of $\mathcal{T}_1$: We first study the mean and variance of $\mathcal{T}_1$ for SFLOCM-DEW scheme under the $\mathcal{H}_0$ hypothesis. Lemma 1 is presented as follows.

Lemma 1: Under $\mathcal{H}_0$, the mean μ_{10} and variance σ_{10}^2 of $\hat{g}_{mm}$ can be given by

$$\begin{aligned} \mu_{10} &= \mathbb{E}\{\hat{g}_{mm}|\mathcal{H}_0\} \\ &= C(b,\alpha)\gamma^{b/\alpha}, \end{aligned} \tag{8}$$

and

$$\begin{aligned} \sigma_{10}^2 &= \mathbb{D}\{\hat{g}_{mm}|\mathcal{H}_0\} \\ &= \frac{1}{K}\left\{C(2b,\alpha)\gamma^{2b/\alpha} - \left(C(b,\alpha)\gamma^{b/\alpha}\right)^2\right\}, \end{aligned} \tag{9}$$

where $C(b,\alpha) = \frac{2^{b+1}\Gamma\left(\frac{b+1}{2}\right)\Gamma(-b/\alpha)}{\alpha\sqrt{\pi}\Gamma(-b/2)}$, $\Gamma(\alpha) = \int_0^\infty x^{\alpha-1}e^{-x}dx$.

Proof: Appendix A. ∎

Next, the detection statistic $\mathcal{T}_1$ can be expressed as

$$\begin{aligned} \mathcal{T}_1 &= \sum_{m=1}^{M}\sum_{n\neq m}^{M} \frac{\hat{g}_{nn} - \mu_{10}}{\sigma_{10}}\hat{g}_{mm} \\ &= \sum_{m=1}^{M} \mathfrak{T}_m, \end{aligned} \tag{10}$$

where $\mathfrak{T}_m = \sum_{n\neq m}^{M} \frac{\hat{g}_{nn}-\mu_{10}}{\sigma_{10}}\hat{g}_{mm}$.

The mean $\mathbb{E}\{\mathfrak{T}_m|\mathcal{H}_0\}$ and variance $\mathbb{D}\{\mathfrak{T}_m|\mathcal{H}_0\}$ of $\mathfrak{T}_m$ under $\mathcal{H}_0$ can be obtained as

$$\begin{aligned} \mathbb{E}\{\mathfrak{T}_m|\mathcal{H}_0\} &= \mathbb{E}\left\{\sum_{n\neq m}^{M}\frac{\hat{g}_{nn}-\mu_{10}}{\sigma_{10}}\hat{g}_{mm}\right\} \\ &= \frac{1}{\sigma_{10}}\mathbb{E}\left\{\sum_{n\neq m}^{M}\left(\hat{g}_{nn}\hat{g}_{mm} - \mu_{10}\hat{g}_{mm}\right)\right\} \\ &= 0, \end{aligned} \tag{11}$$

and

$$\begin{aligned} \mathbb{E}\{\mathfrak{T}_m^2|\mathcal{H}_0\} &= \mathbb{E}\left\{\left(\sum_{n\neq m}^{M}\frac{\hat{g}_{nn}-\mu_{10}}{\sigma_{01}}\hat{g}_{mm}\right)^2\right\} \\ &= \frac{1}{\sigma_{10}^2}\sum_{n\neq m}^{M}\mathbb{E}\{\hat{g}_{nn}\hat{g}_{mm} - \mu_{10}\hat{g}_{mm}\}^2 \\ &= \frac{1}{\sigma_{10}^2}\sum_{n\neq m}^{M}\left(\mathbb{E}\{\hat{g}_{nn}^2\}\mathbb{E}\{\hat{g}_{mm}^2\} + \mu_{10}^2\mathbb{E}\{\hat{g}_{mm}^2\}\right. \\ &\quad \left. -2\mu_{10}\mathbb{E}\{\hat{g}_{nn}\}\mathbb{E}\{\hat{g}_{mm}^2\}\right). \end{aligned} \tag{12}$$

Assuming that $\hat{g}_{mm}$ approaches Gaussian distributions, it can be easily verified under $\mathcal{H}_0$ that

$$\mathbb{E}\left\{\left(\frac{\hat{g}_{mm}-\mu_{10}}{\sigma_{10}}\right)^2\right\}=1. \tag{13}$$

Thus, $\mathbb{E}\left\{\mathfrak{T}_m^2\,|\mathcal{H}_0\right\}$ can be rewritten as

$$\begin{aligned}\mathbb{E}\left\{\mathfrak{T}_m^2\,|\mathcal{H}_0\right\}&=\frac{1}{\sigma_{10}^2}\sum_{n\neq m}^{M}\left(\mathbb{E}\left\{\hat{g}_{nn}^2\right\}\mathbb{E}\left\{\hat{g}_{mm}^2\right\}\right.\\&\left.+\mu_{10}^2\mathbb{E}\{\hat{g}_{mm}^2\}-2\mu_{10}\mathbb{E}\left\{\hat{g}_{nn}\right\}\mathbb{E}\left\{\hat{g}_{mm}^2\right\}\right)\\&=(M-1)\,\mathbb{E}\left(\hat{g}_{mm}^2\right).\end{aligned} \tag{14}$$

Using (11) and (14), the variance of $\mathfrak{T}_m$ can be expressed as

$$\begin{aligned}\mathbb{D}\left\{\mathfrak{T}_m\,|\mathcal{H}_0\right\}&=\mathbb{E}\left\{\mathfrak{T}_m^2\,|\mathcal{H}_0\right\}-\mathbb{E}^2\left\{\mathfrak{T}_m\,|\mathcal{H}_0\right\}\\&=(M-1)\,\mathbb{E}\left(\hat{g}_{mm}^2\right).\end{aligned} \tag{15}$$

Recall that $\mathcal{T}_1=\sum_{m=1}^{M}\mathfrak{T}_m$, the mean and variance of the detection statistic $\mathcal{T}_1$ can be calculated as

$$\mathbb{E}\left\{\mathcal{T}_1\,|\mathcal{H}_0\right\}=\mathbb{E}\left\{\sum_{m=1}^{M}\sum_{n\neq m}^{M}\frac{\hat{g}_{nn}-\mu_{10}}{\sigma_{10}}\hat{g}_{mm}\right\}=0, \tag{16}$$

$$\begin{aligned}\mathbb{D}\left\{\mathcal{T}_1\,|\mathcal{H}_0\right\}&=\mathbb{D}\left\{\sum_{m=1}^{M}\mathfrak{T}_m\right\}\\&=\sum_{m=1}^{M}\mathbb{D}\left\{\mathfrak{T}_m\,|\mathcal{H}_0\right\}+(M-1)^2\,\mathbb{C}(\mathfrak{T}_i,\mathfrak{T}_j),\end{aligned} \tag{17}$$

where $\mathbb{C}\left(\mathfrak{T}_i,\mathfrak{T}_j\right)$ denotes the covariance of any two random variables in $\mathfrak{T}_m\,(m=1,2,....i,....j,....M)$ under $\mathcal{H}_0$. Since $\mathfrak{T}_i$ and $\mathfrak{T}_j$ are related, and there is a constant a such that $P\left(\mathfrak{T}_i=a+\mathfrak{T}_j\right)=1$, $\left|\rho_{\mathfrak{T}_i,\mathfrak{T}_j}\right|=1$, and $\mathbb{D}\left\{\mathfrak{T}_i\right\}=\mathbb{D}\left\{\mathfrak{T}_j\right\}=\mathbb{D}\left\{\mathfrak{T}_m\,|\mathcal{H}_0\right\}$. Accordingly, $\mathbb{C}\left(\mathfrak{T}_i,\mathfrak{T}_j\right)$ is obtained as

$$\mathbb{C}\left(\mathfrak{T}_i,\mathfrak{T}_j\right)=\rho_{\mathfrak{T}_i,\mathfrak{T}_j}\cdot\sqrt{\mathbb{D}\left\{\mathfrak{T}_i\right\}\cdot\mathbb{D}\left\{\mathfrak{T}_j\right\}}=\mathbb{D}\{\mathfrak{T}_m\,|\mathcal{H}_0\}. \tag{18}$$

Using (18), we can rewrite (17) as

$$\begin{aligned}\mathbb{D}\left\{\mathcal{T}_1\,|\mathcal{H}_0\right\}&=\sum_{m=1}^{M}\mathbb{D}\left\{\mathfrak{T}_m\,|\mathcal{H}_0\right\}+(M-1)^2\,\mathbb{C}\left(\mathfrak{T}_i,\mathfrak{T}_j\right)\\&\simeq M\mathbb{D}\left\{\mathfrak{T}_m\,|\mathcal{H}_0\right\}+(M-1)^2\,\mathbb{D}\{\mathfrak{T}_m\,|\mathcal{H}_0\}.\end{aligned} \tag{19}$$

Using the central limit theorem (CLT), when $M\times K$ is large enough, the PDF of $\mathcal{T}_1$ under $\mathcal{H}_0$ can be approximated as a Gaussian distribution with a mean $\mathbb{E}\left\{\mathcal{T}_1\,|\mathcal{H}_0\right\}$ and a variance $\mathbb{D}\left\{\mathcal{T}_1\,|\mathcal{H}_0\right\}$. Therefore, the false alarm probability of $\mathcal{T}_1$ can be expressed as

$$\begin{aligned}P_{f_a}&=P\left(\mathcal{T}_1>\psi_1\,|\mathcal{H}_0\right)\\&=\mathbb{Q}\left(\frac{\psi_1-\mathbb{E}\left\{\mathcal{T}_1\,|\mathcal{H}_0\right\}}{\sqrt{\mathbb{D}\left\{\mathcal{T}_1\,|\mathcal{H}_0\right\}}}\right),\end{aligned} \tag{20}$$

where $\mathbb{Q}$ is called the right tail function of the standard normal distribution with $\mathbb{Q}(x)=\int_x^\infty\frac{1}{\sqrt{2\pi}}e^{-\frac{t^2}{2}}dt$.

Substituting (16) and (19) into (20), the detection threshold can be calculated as

$$\psi_1=\sqrt{\mathbb{D}\left\{\mathcal{T}_1\,|\mathcal{H}_0\right\}}\mathbb{Q}^{-1}\left(P_{f_a}\right)+\mathbb{E}\left\{\mathcal{T}_1\,|\mathcal{H}_0\right\}, \tag{21}$$

where $\mathbb{Q}^{-1}\left(P_{f_a}\right)$ denotes the inverse function of the $\mathbb{Q}$ function.

2) Detection probability of $\mathcal{T}_2$: Consider the mean and variance of $\mathcal{T}_1$ under $\mathcal{H}_1$. We first present Lemma 2.

Lemma 2: Under $\mathcal{H}_1$, the mean and variance of the diagonal elements in the SFLOCM can be derived as

$$\begin{aligned}\mu_{11}&=\mathbb{E}\left\{\hat{g}_{mm}\,|\mathcal{H}_1\right\}\\&\simeq\mu_{10}+\frac{b(b-1)}{2}|h_m|^2\sigma_s^2C(b-2,\alpha)\gamma^{(b-2)/\alpha},\end{aligned} \tag{22}$$

and

$$\begin{aligned}\sigma_{11}^2&=\mathbb{D}\left\{\hat{g}_{mm}\,|\mathcal{H}_1\right\}\\&=\frac{1}{K}\left(C(2b,\alpha)\gamma^{2b/\alpha}\right.\\&\left.+b(2b-1)|h_m|^2\sigma_s^2C(2b-2,\alpha)\gamma^{(2b-2)/\alpha}-\mu_{11}^2\right).\end{aligned} \tag{23}$$

Proof: Appendix B. ∎

For simplification, we first calculate the mean of $\mathfrak{T}_m=\sum_{n\neq m}^{M}\frac{\hat{g}_{nn}-\mu_{10}}{\sigma_{10}}\hat{g}_{mm}$ under $\mathcal{H}_1$ as

$$\begin{aligned}\mathbb{E}\left\{\mathfrak{T}_m\,|\mathcal{H}_1\right\}&=\mathbb{E}\left\{\sum_{n\neq m}^{M}\frac{\hat{g}_{nn}-\mu_{10}}{\sigma_{10}}\hat{g}_{mm}\right\}\\&=\frac{1}{\sigma_{10}}\mathbb{E}\left\{\sum_{n\neq m}^{M}\left(\hat{g}_{nn}\hat{g}_{mm}-\mu_{10}\hat{g}_{mm}\right)\right\}.\end{aligned} \tag{24}$$

Using (24), the variance of $\mathfrak{T}_m$ under $\mathcal{H}_1$ can be expressed as in (25), shown at the bottom of the page, where the term $\mathbb{C}\left(\mathfrak{J}_i,\mathfrak{J}_j\right)$ corresponds to the covariance of any two random variables in $\mathfrak{J}_n=(\hat{g}_{nn}-\mu_{10})$ under $\mathcal{H}_1$.

$$\begin{aligned}\mathbb{D}\left\{\mathfrak{T}_m|\mathcal{H}_1\right\}&=\mathbb{E}\left\{\mathfrak{T}_m^2\,|\mathcal{H}_1\right\}-\mathbb{E}^2\left\{\mathfrak{T}_m|\mathcal{H}_1\right\}\\&=\mathbb{E}\left\{\left(\sum_{n\neq m}^{M}\frac{\hat{g}_{nn}-\mu_{10}}{\sigma_{10}}\hat{g}_{mm}\right)^2\right\}-\mathbb{E}^2\left\{\sum_{n\neq m}^{M}\frac{\hat{g}_{nn}-\mu_{10}}{\sigma_{10}}\hat{g}_{mm}\right\}\\&=\frac{1}{\sigma_{10}^2}\left(\sum_{n\neq m}^{M}\mathbb{E}(\hat{g}_{nn}\hat{g}_{mm}-\mu_{10}\hat{g}_{mm})^2+\mathbb{C}\left(\mathfrak{J}_i,\mathfrak{J}_j\right)-\mathbb{E}^2\left\{\sum_{n\neq m}^{M}\left(\hat{g}_{nn}\hat{g}_{mm}-\mu_{10}\hat{g}_{mm}\right)\right\}\right)\end{aligned} \tag{25}$$

Since $\mathcal{T}_1 = \sum_{m=1}^{M} \mathfrak{T}_m$, the mean and variance of $\mathcal{T}_1$ under H_1 can be expressed as

$$\mathbb{E}\left\{\mathcal{T}_1|\mathcal{H}_1\right\} \approx \sum_{m=1}^{M} \mathbb{E}\left\{\mathfrak{T}_m|\mathcal{H}_1\right\}, \tag{26}$$

$$\mathbb{D}\{\mathcal{T}_1|\mathcal{H}_1\} \approx \sum_{m=1}^{M} \mathbb{D}\{\mathfrak{T}_m|\mathcal{H}_1\} + M(M-1)\mathbb{C}\left(\mathfrak{T}_i, \mathfrak{T}_j\right), \tag{27}$$

where $\mathbb{C}\left(\mathfrak{T}_i, \mathfrak{T}_j\right)$ denotes the covariance of any two random variables in $\mathfrak{T}_m$ under $\mathcal{H}_1$. When $M \times K$ goes to infinity, using CLT, the $\mathcal{T}_1|\,\mathcal{H}_1$ can be approximated as a Gaussian distribution. Therefore, the detection probability of $\mathcal{T}_1$ can be expressed as

$$\begin{aligned} P_{d_1} &= P\left(\mathcal{T}_1 > \psi_1\,|\mathcal{H}_1\right) \\ &= \mathbb{Q}\left(\frac{\eta_1 - \sum_{m=1}^{M} \mathbb{E}\left\{\mathfrak{T}_m|\mathcal{H}_1\right\}}{\sqrt{\sum_{m=1}^{M} \mathbb{D}\{\mathfrak{T}_m|\mathcal{H}_1\} + M(M-1)\mathbb{C}\left(\mathfrak{T}_i, \mathfrak{T}_j\right)}}\right), \end{aligned} \tag{28}$$

where P_{d_1} is dependent of M, μ_{10}, μ_{11}, σ_{10}^2 and σ_{11}^2.

B. Performance of SFLOCM-ODEW Scheme

1) False alarm probability and detection threshold of $\mathcal{T}_2$:

Lemma 3: Under $\mathcal{H}_0$, the mean and variance of the off-diagonal element $\hat{g}_{mn}$ in the SFLOCM can be derived as

$$\mu_{20} = C^2\left(b/2, \alpha\right)\gamma^{b/\alpha}, \tag{29}$$

and

$$\sigma_{20}^2 = \frac{1}{K}\left(C\left(2b, \alpha\right)\gamma^{2b/\alpha} - \left(C^2\left(b/2, \alpha\right)\gamma^{b/\alpha}\right)^2\right). \tag{30}$$

Proof: Appendix C. ∎

Let $\mathfrak{T}_{mp} = g_{mm} \sum_{q\neq p\neq m}^{M} \frac{\hat{g}_{pq}-u_{20}}{\sigma_{20}}$. The detection statistic $\mathcal{T}_2$ can be rewritten as

$$\begin{aligned} \mathcal{T}_2 &= \sum_{m=1}^{M} \hat{g}_{mm} \sum_{\substack{p=1 \\ p\neq m}}^{M} \sum_{\substack{q=1 \\ q\neq p\neq m}}^{M} \frac{\hat{g}_{pq} - \mu_{20}}{\sigma_{20}} \\ &= \sum_{m=1}^{M} \sum_{\substack{p=1 \\ p\neq m}}^{M} \mathfrak{T}_{mp}. \end{aligned} \tag{31}$$

Next, we calculate the first and second-order moments of $\mathfrak{T}_{mp}$ under $\mathcal{H}_0$ as

$$\begin{aligned} \mathbb{E}\left\{\mathfrak{T}_{mp}\,|\mathcal{H}_0\right\} &= \mathbb{E}\left\{\sum_{q\neq p\neq m}^{M} \frac{\hat{g}_{pq} - \mu_{20}}{\sigma_{20}}\hat{g}_{mm}\right\} \\ &= \frac{1}{\sigma_{20}}\mathbb{E}\left\{\sum_{q\neq p\neq m}^{M} (\hat{g}_{pq} - \mu_{20})\hat{g}_{mm}\right\} \\ &= \frac{1}{\sigma_{20}} \sum_{q\neq p\neq m}^{M} \left(\mathbb{E}\left\{\hat{g}_{mm}\right\}\mathbb{E}\left\{\hat{g}_{pq}\right\} - \mu_{20}\mathbb{E}\left\{\hat{g}_{mm}\right\}\right) \\ &= 0, \end{aligned} \tag{32}$$

and

$$\begin{aligned} \mathbb{E}\left\{\mathfrak{T}_{mp}^2\,|\mathcal{H}_0\right\} &= \mathbb{E}\left\{\left(\sum_{q\neq p\neq m}^{M} \frac{\hat{g}_{pq} - \mu_{20}}{\sigma_{20}}\hat{g}_{mm}\right)^2\right\} \\ &= \frac{1}{\sigma_{20}^2} \sum_{q\neq p\neq m}^{M} E(\hat{g}_{pq}\hat{g}_{mm} - \mu_{20}\hat{g}_{mm})^2. \end{aligned} \tag{33}$$

Using (32) and (33), the variance of $\mathfrak{T}_z$ can be obtained as

$$\begin{aligned} \mathbb{D}\left\{\mathfrak{T}_{mp}\,|\mathcal{H}_0\right\} &= \mathbb{E}\left\{\mathfrak{T}_{mp}^2\,|\mathcal{H}_0\right\} - \mathbb{E}^2\left\{\mathfrak{T}_{mp}\,|\mathcal{H}_0\right\} \\ &= \mathbb{E}\left\{\mathfrak{T}_{mp}^2\,|\mathcal{H}_0\right\}. \end{aligned} \tag{34}$$

Subsequently, let $\tilde{\mathfrak{T}}_z = \sum_{p=1, p\neq m}^{M} \mathfrak{T}_{mp}$, the mean $\mathbb{E}\left\{\tilde{\mathfrak{T}}_z\,|\mathcal{H}_0\right\}$ and variance $\mathbb{D}\left\{\tilde{\mathfrak{T}}_z\,|\mathcal{H}_0\right\}$ are shown (35) and (36) at the bottom of the page. In (36), $\mathbb{C}\left(\mathfrak{T}_{mi}, \mathfrak{T}_{mj}\right)$ is the covariance of any two random variables in $\mathfrak{T}_{mp}\,(p = 1, 2, ...i, ...j, ...M)$ under $\mathcal{H}_1$. Due to $\mathfrak{T}_{mi}$ and $\mathfrak{T}_{mj}$ are related, and there is a constant a such that $P\left(\mathfrak{T}_{mj} = a + \mathfrak{T}_{mj}\right) = 1$, then $\left|\rho_{\mathfrak{T}_{mi}, \mathfrak{T}_{mj}}\right| = 1$, and $\mathbb{D}\left\{\mathfrak{T}_{mi}\right\} = \mathbb{D}\left\{\mathfrak{T}_{mj}\right\} = \mathbb{D}\left\{\mathfrak{T}_{mp}\,|\mathcal{H}_0\right\}$. Obviously, $\mathbb{C}\left(\mathfrak{T}_{mi}, \mathfrak{T}_{mj}\right) = \rho_{\mathfrak{T}_{mi}, \mathfrak{T}_{mj}} \cdot \sqrt{\mathbb{D}\left\{\mathfrak{T}_{mi}\right\}\mathbb{D}\left\{\mathfrak{T}_{mj}\right\}} = \mathbb{D}\left\{\mathfrak{T}_{mp}\,|\mathcal{H}_0\right\}$. Consequently, (36) can be simplified as

$$\begin{aligned} \mathbb{D}\left\{\tilde{\mathfrak{T}}_z\,|\mathcal{H}_0\right\} &= \mathbb{D}\left\{\sum_{\substack{p=1 \\ p\neq m}}^{M} \mathfrak{T}_{mp}\right\} \\ &\simeq (M-1)(M-2)\,\mathbb{D}\left\{\mathfrak{T}_{mp}\,|\mathcal{H}_0\right\}. \end{aligned} \tag{37}$$

$$\mathbb{E}\left\{\tilde{\mathfrak{T}}_z\,|\mathcal{H}_0\right\} = \mathbb{E}\left\{\hat{g}_{mm} \sum_{\substack{p=1 \\ p\neq m}}^{M} \sum_{\substack{q=1 \\ q\neq p\neq m}}^{M} \frac{\hat{g}_{pq} - \mu_{20}}{\sigma_{20}}\right\} = 0 \tag{35}$$

$$\mathbb{D}\left\{\tilde{\mathfrak{T}}_z\,|\mathcal{H}_0\right\} = \mathbb{D}\left\{\sum_{\substack{p=1 \\ p\neq m}}^{M} \mathfrak{T}_{mp}\right\} = \sum_{\substack{p=1 \\ p\neq m}}^{M} \mathbb{D}\left\{\mathfrak{T}_{mp}\,|\mathcal{H}_0\right\} + (M-2)^2\,\mathbb{C}\left(\mathfrak{T}_{mi}, \mathfrak{T}_{mj}\right) \tag{36}$$

From the above, the mean and variance of the detection statistics $\mathcal{T}_2$ can be derived as

$$\mathbb{E}\left\{\mathcal{T}_2\left|\mathcal{H}_0\right.\right\} \simeq \sum_{m=1}^{M} \mathbb{D}\left\{\tilde{\mathfrak{T}}_z|\mathcal{H}_0\right\} = 0, \tag{38}$$

$$\mathbb{D}\{\mathcal{T}_2|\mathcal{H}_0\} \simeq \sum_{m=1}^{M} \mathbb{D}\left\{\tilde{\mathfrak{T}}_z|\mathcal{H}_0\right\} + (M-1)^2 \mathbb{C}\left(\tilde{\mathfrak{T}}_i, \tilde{\mathfrak{T}}_j\right), \tag{39}$$

where $\mathbb{C}\left(\tilde{\mathfrak{T}}_i, \tilde{\mathfrak{T}}_j\right)$ denotes the covariance of any two random variables in $\tilde{\mathfrak{T}}_z$ $(z = 1, 2, ...i, ...j, ...M)$ under $\mathcal{H}_0$. Using the CLT, the detection statistics $\mathcal{T}_2$ under $\mathcal{H}_0$ can be approximated as a Gaussian distribution when $M \times K$ is large enough. Therefore, the false alarm probability of $\mathcal{T}_2$ can be expressed as

$$\begin{aligned} P_{f_a} &= P\left(\mathcal{T}_2 > \psi_2 \left|\mathcal{H}_0\right.\right) \\ &= \mathbb{Q}\left(\frac{\eta_2 - \mathbb{E}\left\{\mathcal{T}_2\left|\mathcal{H}_0\right.\right\}}{\sqrt{\mathbb{D}\left\{\mathcal{T}_2\left|\mathcal{H}_0\right.\right\}}}\right). \end{aligned} \tag{40}$$

Accordingly, if the false-alarm probability is fixed of P_{f_a}, the detection threshold ψ_2 can be determined as

$$\psi_2 = \sqrt{\mathbb{D}\left\{\mathcal{T}_2\left|\mathcal{H}_0\right.\right\}}\mathbb{Q}^{-1}(P_{f_a}) - \mathbb{E}\left\{\mathcal{T}_2\left|\mathcal{H}_0\right.\right\}. \tag{41}$$

2) Detection probability of $\mathcal{T}_2$: We first present the following Lemma 4.

Lemma 4: Under $\mathcal{H}_1$, the mean μ_{21} and variance σ_{21}^2 of $\hat{g}_{pq}$ can be derived as

$$\begin{aligned} \mu_{21} \simeq \Big(&C(b/2,\alpha)\gamma^{(b/2)/\alpha} \\ &+ \frac{b/2(b/2-1)}{2}|h_m|^2\sigma_s^2 C(b/2-2,\alpha)\gamma^{(b/2-2)/\alpha}\Big)^2, \end{aligned} \tag{42}$$

and

$$\sigma_{21}^2 \simeq \frac{1}{K}\left(\mu_{11}^2 - \mu_{21}^2\right). \tag{43}$$

Proof: Appendix D. ∎

Recall that $\mathcal{T}_2 = \sum_{m=1}^{M} \mathfrak{T}_z$ and $\mathfrak{T}_z = \hat{g}_{mm} \sum_{\substack{p=1 \\ p\neq m}}^{M} \sum_{\substack{q=1 \\ q\neq p\neq m}}^{M} \frac{\hat{g}_{pq}-\mu_{20}}{\sigma_{20}}$, under $\mathcal{H}_1$, the mean $\mathbb{E}\left\{\mathfrak{T}_z\left|\mathcal{H}_1\right.\right\}$ can be calculated as

$$\begin{aligned} \mathbb{E}\left\{\mathfrak{T}_z\left|\mathcal{H}_1\right.\right\} &= \mathbb{E}\left\{\hat{g}_{mm} \sum_{\substack{p=1 \\ p\neq m}}^{M} \sum_{\substack{q=1 \\ q\neq p\neq m}}^{M} \frac{\hat{g}_{pq}-\mu_{20}}{\sigma_{20}}\right\} \\ &= \frac{1}{\sigma_{20}}\mathbb{E}\left\{\sum_{\substack{p=1 \\ p\neq m}}^{M} \sum_{\substack{q=1 \\ q\neq p\neq m}}^{M} \hat{g}_{mm}\left(\hat{g}_{pq}-\mu_{20}\right)\right\} \\ &= \frac{1}{\sigma_{20}} \sum_{\substack{p=1 \\ p\neq m}}^{M} \sum_{\substack{q=1 \\ q\neq p\neq m}}^{M} \mathbb{E}\left\{\hat{g}_{mm}\left(\hat{g}_{pq}-\mu_{20}\right)\right\}. \end{aligned} \tag{44}$$

The variance $\mathbb{D}\left\{\mathfrak{T}_z\left|\mathcal{H}_1\right.\right\}$ can be expressed as in (45) at the bottom of the page, where $\mathbb{C}\left(\mathfrak{J}_{ij}, \mathfrak{J}_{kl}\right)$ represents the covariance of any two random variables in $\mathfrak{J}_{pq} = (\hat{g}_{pq}\hat{g}_{mm} - \mu_{20}\hat{g}_{mm})$.

Using the above, the mean $\mathbb{E}\left\{\mathcal{T}_2\left|\mathcal{H}_1\right.\right\}$ and variance $\mathbb{E}\left\{\mathcal{T}_2\left|\mathcal{H}_1\right.\right\}$ of the detection statistics $\mathcal{T}_2$ can be expressed as

$$\mathbb{E}\left\{\mathcal{T}_2|\mathcal{H}_1\right\} \simeq \sum_{m=1}^{M} \mathbb{E}\left\{\mathfrak{T}_z|\mathcal{H}_1\right\}, \tag{46}$$

$$\mathbb{D}\{\mathcal{T}_2|\mathcal{H}_1\} \simeq \sum_{m=1}^{M} \mathbb{D}\left\{\mathfrak{T}_z|\mathcal{H}_1\right\} + M(M-1)\mathbb{C}\left(\mathfrak{T}_k, \mathfrak{T}_l\right), \tag{47}$$

where $\mathbb{C}\left(\mathfrak{T}_k, \mathfrak{T}_l\right)$ denotes the covariance of any two random variables in $\mathfrak{T}_z$ under $\mathcal{H}_1$.

For sufficiently large $M \times K$, the detection probability P_{d_2} can be approximated as

$$\begin{aligned} P_{d_2} &= P\left(\mathcal{T}_2 > \psi_2 \left|\mathcal{H}_1\right.\right) \\ &= \mathbb{Q}\left(\frac{\psi_2 - \mathbb{E}\left\{\mathcal{T}_2|H_1\right\}}{\sqrt{\mathbb{D}\left\{\mathcal{T}_2|\mathcal{H}_1\right\}}}\right) \\ &= \mathbb{Q}\left(\frac{\psi_2 - \sum_{m=1}^{M} \mathbb{E}\left\{\mathfrak{T}_z|\mathcal{H}_1\right\}}{\sqrt{\sum_{m=1}^{M} \mathbb{D}\{\mathfrak{T}_z|\mathcal{H}_1\} + M(M-1)\mathbb{C}(\mathfrak{T}_k, \mathfrak{T}_l)}}\right) \end{aligned} \tag{48}$$

where P_{d2} is related to values M, μ_{10}, μ_{11}, μ_{20}, μ_{21}, σ_{10}^2, σ_{11}^2, σ_{20}^2 and σ_{21}^2.

$$\begin{aligned} \mathbb{D}\left\{\mathfrak{T}_z|H_1\right\} &= \mathbb{E}\left\{\mathfrak{T}_z^2|H_1\right\} - \mathbb{E}^2\left\{\mathfrak{T}_z|H_1\right\} \\ &= \mathbb{E}\left\{\left(\hat{g}_{mm} \sum_{\substack{p=1 \\ p\neq m}}^{M} \sum_{\substack{q=1 \\ q\neq p\neq m}}^{M} \frac{\hat{g}_{pq}-\mu_{20}}{\sigma_{20}}\right)^2\right\} - \mathbb{E}^2\left\{\hat{g}_{mm} \sum_{\substack{p=1 \\ p\neq m}}^{M} \sum_{\substack{q=1 \\ q\neq p\neq m}}^{M} \frac{\hat{g}_{pq}-\mu_{20}}{\sigma_{20}}\right\} \\ &= \frac{1}{\sigma_{20}^2}\left(\sum_{\substack{p=1 \\ p\neq m}}^{M} \sum_{\substack{q=1 \\ q\neq p\neq m}}^{M} \mathbb{E}\left\{\left(\hat{g}_{mm}\hat{g}_{pq} - \hat{g}_{mm}\mu_{20}\right)^2\right\} + \mathbb{C}\left(\mathfrak{J}_{ij}, \mathfrak{J}_{kl}\right) - \left(\sum_{\substack{p=1 \\ p\neq m}}^{M} \sum_{\substack{q=1 \\ q\neq p\neq m}}^{M} \mathbb{E}\left\{\hat{g}_{mm}\left(\hat{g}_{pq}-\mu_{20}\right)\right\}\right)^2\right) \end{aligned} \tag{45}$$

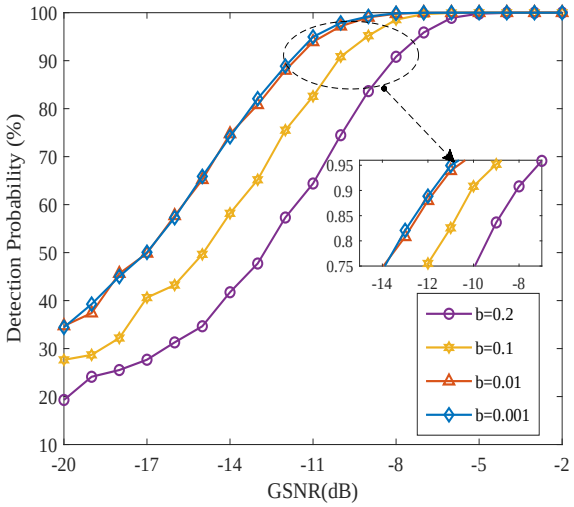

Fig. 2. Detection probability of the SFLOCM-DEW scheme versus GSNR at $P_{fa} = 0.1$ for different values of b.

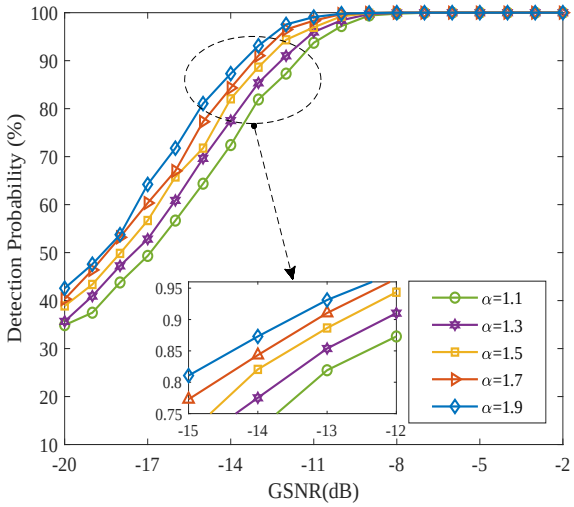

Fig. 4. Detection probability of the SFLOCM-DEW scheme versus GSNR at $P_{fa} = 0.1$ for different values of α.

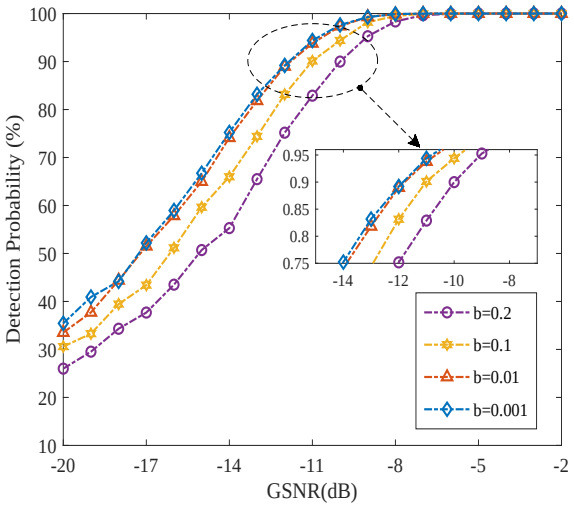

Fig. 3. Detection probability of the SFLOCM-ODEW scheme versus GSNR at $P_{fa} = 0.1$ for different values of b.

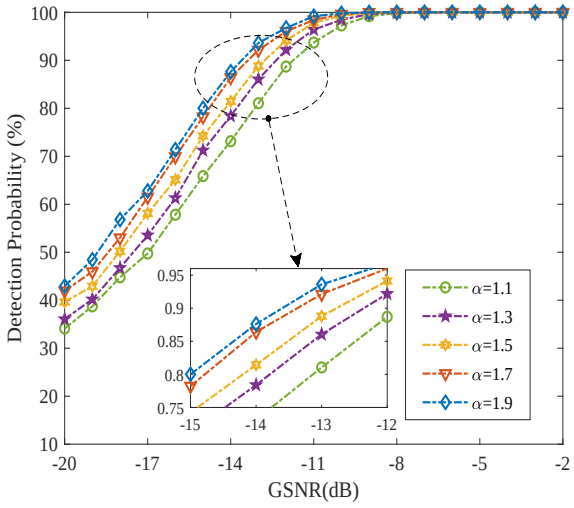

Fig. 5. Detection probability of the SFLOCM-ODEW scheme versus GSNR at $P_{fa} = 0.1$ for different values of α.

V. Simulation Results and Analysis

To verify the performance of the two proposed algorithms, simulations are conducted in this section. It is assumed that the PU signal is a QAM signal, and the noise follows a symmetric $S\alpha S$ distribution. The the false alarm probability is $P_{fa} = 0.1$. All the curves are averaged over 8000 runs.

The detection performances of the two spectrum sensing schemes for different orders ($b = 0.2, 0.1, 0.01, 0.001$) are shown in Fig. 2 and Fig. 3, respectively. We consider that the number of receiving antennas is $M = 5$, and the characteristic exponent is $\alpha = 1.1$. It can be seen from these figures that the detection probability increases when the orders b decreases in the same GSNR regime. For example, as b decreases from 0.2 to 0.01, the detection probability increases from 75% to 95% at GSNR=-10dB in Fig. 2. Furthermore, from Figs. 2-3, it can be seen that the detection performance of the proposed schemes does not change with b when $b < 0.01$. Thus, b can be set to 0.01 in subsequent simulation experiments.

Figs. 4-5 respectively present the effect of the characteristic exponent α for the two proposed spectrum sensing schemes. We also assume that the number of receiving antennas is $M = 5$, and the number of samples $K = 100$. It is observed that the detection probability of two schemes degrades with the decrease of the characteristic exponent α. For example, when GSNR=-12dB, the SFLOCM-ODEW scheme close to 97% detection probability at $\alpha = 1.9$, but approximately 87% detection probability at $\alpha = 1.1$. As a summary, since the decreasing value of the characteristic exponent can make the detection statistics deviate from the theoretical value, which can cause performance degradation with the decrease of α values.

Figs. 6-7 illustrate the detection probability for different receiving antennas numbers ($M = 5, 6, 7, 8, 9, 10$) versus the

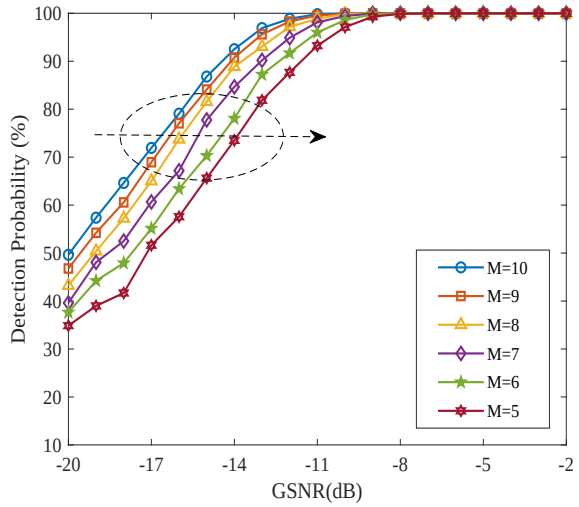

Fig. 6. Detection probability of the SFLOCM-DEW detector versus GSNR at $P_{fa} = 0.1$ for different antenna numbers M.

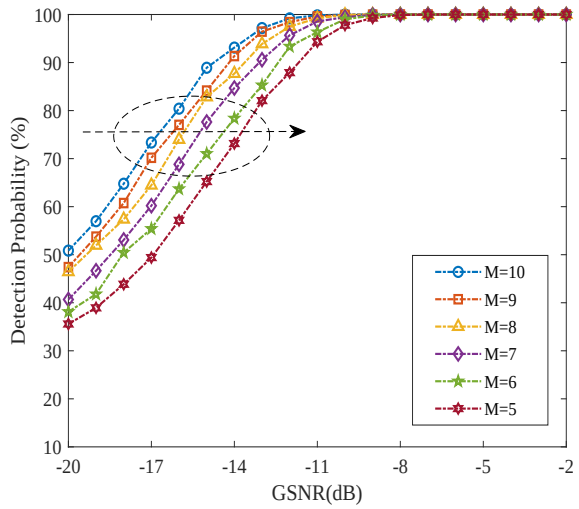

Fig. 7. Detection probability of the SFLOCM-ODEW detector versus GSNR at $P_{fa} = 0.1$ for different antenna numbers M.

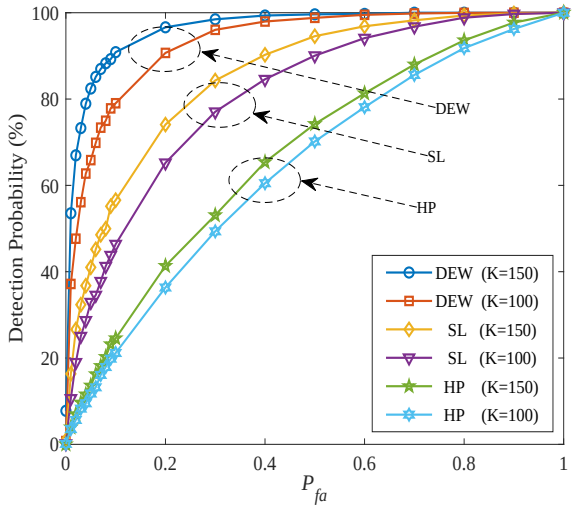

Fig. 8. ROC curves of the SFLOCM-DEW and different detectors at GSNR=-16dB and $\alpha = 1.1$ for different samples K.

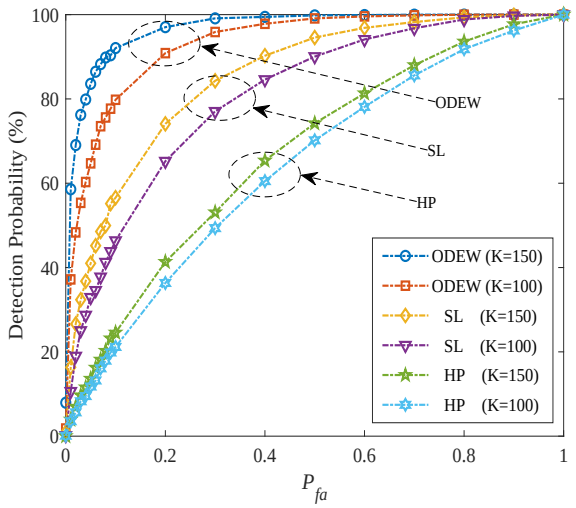

Fig. 9. ROC curves of the SFLOCM-ODEW and different detectors at GSNR=-16dB and $\alpha = 1.1$ for different samples K.

GSNR at $b = 0.01$ and $\alpha = 1.1$. It is observed that the detection probability increases with the number of receiving antennas M. From Fig. 6, we observe that, for given GSNR=-14, the performance of the proposed detector is close to 73% when $M = 5$, and close to 93% when $M = 10$. This is mainly because with the increase of the number of antennas, the sample covariance matrix approach the ideal covariance matrix and the detection statistics are close to the theoretical distribution, so that the detection performance increases with the increase of the number of antennas.

Finally, the Receiver Operating Characteristics (ROC) is employed to evaluate the proposed schemes. In Figs. 8-9, the detection performance of the proposed schemes is compared with that of the Hole Puncher-based (HP) detector and the Soft Limiter-based (SL) detector. We set the basic simulation parameters as $\alpha = 1.1$, $M = 10$, $b = 0.01$ and GSNR=-16dB. It can be seen that the proposed schemes achieve better performance than the HP detector and the SL detector. Form Fig. 9, we observed that, compared to HP detector and SL detector, the proposed schemes improves the detection accuracy by 50% and 30%, respectively. In addition, we can also find that the detection performance of the proposed schemes significantly improves when the number of samples is increased from 100 to 150. Moreover, we analyze the computation complexity. Given the number of samples K and antennas M, the computational complexity of the SFLOCM-DEW and SFLOCM-ODEW scheme are $O\left(KM^2\right)$ and $O\left(KM^3\right)$, the computational complexity of the HP detector is $O\left(KM\right)$, and the computational complexity of the SL detector is $O\left(KM\right)$.

VI. Conclusion

In this paper, two spectrum sensing schemes have been proposed using the fractional low-order covariance matrix to

combat the alpha-stable noise, namely SFLOCM-DEW detector and SFLOCM-ODEW detector. The relationship between the detection threshold and the false alarm probability of the two proposed schemes have been derived. Besides, the approximate analytical expressions of the detection probability have been analyzed. Finally, simulation results have shown that the proposed two schemes have achieved reliable detection performance in the presence of α-stable impulsive noise. Compared with existing methods, these proposed schemes have provided higher performance in the case of a small GSNR. Moreover, we have observed from the results that the proposed schemes can offer a large performance gain with the increasing number of samples or antennas under moderate heavy-tailed noise conditions ($1 < \alpha < 2$). In future work, we will focus on developing a convenient and reliable detector for time-varying channels in impulsive noise under unknown noise parameters.

APPENDIX A
PROOF OF LEMMA 1

Under $\mathcal{H}_0$, the first and second-order moments of the diagonal elements $\hat{g}_{mm}$ in the SFLOCM can be calculated as

$$\begin{aligned}\mu_{10} &= \mathbb{E}\left\{\hat{g}_{mm}\left|\mathcal{H}_0\right.\right\} \\ &= \mathbb{E}\left\{\frac{1}{K}\sum_{k=1}^{K}\left|x_m\left(k\right)\right|^{b/2}\left|x_m^*\left(k\right)\right|^{b/2}\right\} \\ &= \frac{1}{K}\sum_{k=1}^{K}\mathbb{E}\left\{\left|w_m\left(k\right)\right|^{b/2}\left|w_m^*\left(k\right)\right|^{b/2}\right\} \\ &= \frac{1}{K}\sum_{k=1}^{K}\mathbb{E}\left\{\left|w_m\left(k\right)\right|^{b}\right\} \\ &= C\left(b,\alpha\right)\gamma^{b/\alpha},\end{aligned} \tag{49}$$

and

$$\begin{aligned}&\mathbb{E}\left\{\hat{g}_{mm}^2\left|\mathcal{H}_0\right.\right\} \\ =&\mathbb{E}\left\{\left(\frac{1}{K}\sum_{k=1}^{K}\left|x_m\left(k\right)\right|^{b/2}\left|x_m^*\left(k\right)\right|^{b/2}\right)^2\right\} \\ =&\mathbb{E}\left\{\left(\frac{1}{K}\sum_{k=1}^{K}\left|w_m\left(k\right)\right|^{b/2}\left|w_m^*\left(k\right)\right|^{b/2}\right)^2\right\} \\ =&\frac{1}{K^2}\mathbb{E}\left\{\left(\sum_{k=1}^{K}\left|w_m\left(k\right)\right|^{b}\right)^2\right\},\end{aligned} \tag{50}$$

where $C(b,\alpha) = \frac{2^{b+1}\Gamma\left(\frac{b+1}{2}\right)\Gamma(-b/\alpha)}{\alpha\sqrt{\pi}\Gamma(-b/2)}$, $\Gamma(\alpha) = \int_0^\infty x^{\alpha-1}e^{-x}dx$, γ is the dispersion coefficient of the distribution, α is the characteristic exponent of the distribution, and b is the fractional order [27].

Based on (49) and (50), the variance of the $\hat{g}_{mm}$ can be expressed as

$$\begin{aligned}\sigma_{10}^2 =&\mathbb{D}\left\{\hat{g}_{mm}\left|\mathcal{H}_0\right.\right\} \\ =&\mathbb{E}\left\{\hat{g}_{mm}^2\left|\mathcal{H}_0\right.\right\} - \mathbb{E}^2\left\{\hat{g}_{mm}\left|\mathcal{H}_0\right.\right\} \\ =&\frac{1}{K^2}\mathbb{E}\left\{\left(\sum_{k=1}^{K}\left|w_m\left(k\right)\right|^{b}\right)^2\right\} \\ &-\frac{1}{K^2}\left(\sum_{k=1}^{K}\mathbb{E}\left\{\left|w_m\left(k\right)\right|^{b}\right\}\right)^2 \\ =&\frac{1}{K}\left(\mathbb{E}\left\{\left|w_m\left(k\right)\right|^{2b}\right\} - \mathbb{E}^2\left\{\left|w_m\left(k\right)\right|^{b}\right\}\right) \\ =&\frac{1}{K}\left(C\left(2b,\alpha\right)\gamma^{2b/\alpha} - \left(C\left(b,\alpha\right)\gamma^{b/\alpha}\right)^2\right).\end{aligned} \tag{51}$$

APPENDIX B
PROOF OF LEMMA 2

Under $\mathcal{H}_1$, the mean of $\hat{g}_{mm}$ can be calculated as

$$\begin{aligned}\mu_{11} =&\mathbb{E}\left\{\hat{g}_{mm}|\mathcal{H}_1\right\} \\ =&\mathbb{E}\left\{\frac{1}{K}\sum_{k=1}^{K}\left|x_m\left(k\right)\right|^{b/2}\left|x_m^*\left(k\right)\right|^{b/2}\right\} \\ =&\frac{1}{K}\sum_{k=1}^{K}\mathbb{E}\left\{\left|x_m\left(k\right)\right|^{b/2}\left|x_m^*\left(k\right)\right|^{b/2}\right\} \\ =&\frac{1}{K}\sum_{k=1}^{K}\mathbb{E}\left\{\left|x_m\left(k\right)\right|^{b}\right\} \\ =&\frac{1}{K}\sum_{k=1}^{K}\mathbb{E}\left\{\left|h_m s(k) + w_m\left(k\right)\right|^{b}\right\}.\end{aligned} \tag{52}$$

Using the generalized binomial theorem [37], (52) can be rewritten as in (53) at the bottom of the page.

When $|h_m s(k)| \ll |w_m(k)|$ in the assumption of low GSNR, the higher-order terms of $|h_m s(k)|$ can be ignored. Moreover, the mean of $s(k)$ is 0 and the variance of $s(k)$ is σ_s^2. Thus, the mean μ_{11} can be approximated as

$$\begin{aligned}\mu_{11} &\approx \mathbb{E}\left\{|w_m(k)|^b + \frac{b(b-1)}{2!}|h_m s(k)|^2|w_m(k)|^{b-2}\right\} \\ &= \mu_{10} + \frac{b(b-1)}{2}|h_m|^2\mathbb{E}\left\{|s(k)|^2\right\}\mathbb{E}\left\{|w_m(k)|^{b-2}\right\} \\ &= \mu_{10} + \frac{b(b-1)}{2}|h_m|^2\sigma_s^2 C(b-2,\alpha)\gamma^{(b-2)/\alpha}.\end{aligned} \tag{54}$$

Using (54), the variance of $\hat{g}_{mm}$ can be calculated as in (55) at the bottom of the next page.

$$\mu_{11} = \mathbb{E}\left\{|w_m(k)|^b + b\,|h_m s(k)|\,|w_m(k)|^{b-1} + \frac{b(b-1)}{2!}|h_m s(k)|^2|w_m(k)|^{b-2} + \cdots\right\}. \tag{53}$$

APPENDIX C
PROOF OF LEMMA 3

Under $\mathcal{H}_0$, the first and second-order moments of the off-diagonal elements $\hat{g}_{mn}$ in the SFLOCM can be derived as

$$\begin{aligned}\mu_{20} =&\mathbb{E}\left\{\hat{g}_{mn}\left|\mathcal{H}_0\right.\right\}\\ =&\mathbb{E}\left\{\frac{1}{K}\sum_{k=1}^{K}\left|x_m\left(k\right)\right|^{b/2}\left|x_n^*\left(k\right)\right|^{b/2}\right\}\\ =&\mathbb{E}\left\{\frac{1}{K}\sum_{k=1}^{K}\left|w_m\left(k\right)\right|^{b/2}\left|w_n^*\left(k\right)\right|^{b/2}\right\}\\ =&\mathbb{E}^2\left\{\left|w_m\left(k\right)\right|^{b/2}\right\}\\ =&C^2\left(b/2,\alpha\right)\gamma^{b/\alpha},\end{aligned}\tag{56}$$

and

$$\begin{aligned}&\mathbb{E}\left\{\hat{g}_{mn}^2\left|\mathcal{H}_0\right.\right\}\\ =&\mathbb{E}\left\{\left(\frac{1}{K}\sum_{k=1}^{K}\left|x_m\left(k\right)\right|^{b/2}\left|x_n^*\left(k\right)\right|^{b/2}\right)^2\right\}\\ =&\mathbb{E}\left\{\left(\frac{1}{K}\sum_{k=1}^{K}\left|w_m\left(k\right)\right|^{b/2}\left|w_n^*\left(k\right)\right|^{b/2}\right)^2\right\}\\ =&\frac{1}{K^2}\mathbb{E}\left\{\left(\sum_{k=1}^{K}\left|w_m\left(k\right)\right|^{b/2}\left|w_n^*\left(k\right)\right|^{b/2}\right)^2\right\}.\end{aligned}\tag{57}$$

Using (31), we may obtain the variance of $\hat{g}_{mn}$ under $\mathcal{H}_0$ as

$$\begin{aligned}\sigma_{20}^2 =&\mathbb{E}\left\{\hat{g}_{mn}^2\left|\mathcal{H}_0\right.\right\}-\mathbb{E}^2\left\{\hat{g}_{mn}\left|\mathcal{H}_0\right.\right\}\\ =&\frac{1}{K^2}\mathbb{E}\left\{\left(\sum_{k=1}^{K}\left|w_m\left(k\right)\right|^{b/2}\left|w_n^*\left(k\right)\right|^{b/2}\right)^2\right\}\\ &-\mathbb{E}^2\left\{\frac{1}{K}\sum_{k=1}^{K}\left|w_m\left(k\right)\right|^{b/2}\left|w_n^*\left(k\right)\right|^{b/2}\right\}\\ =&\frac{1}{K}\left(\mathbb{E}\left\{\left|w_m\left(k\right)\right|^{2b}\right\}-\mathbb{E}^4\left\{\left|w_m\left(k\right)\right|^{b/2}\right\}\right)\\ =&\frac{1}{K}\left(C\left(2b,\alpha\right)\gamma^{2b/\alpha}-\left(C\left(b/2,\alpha\right)\gamma^{b/2\alpha}\right)^2\right).\end{aligned}\tag{58}$$

APPENDIX D
PROOF OF LEMMA 4

Similarly, we first calculate the mean of the off-diagonal elements $\hat{g}_{mn}$ under $\mathcal{H}_1$ as

$$\begin{aligned}\mu_{21} =&\mathbb{E}\left\{\hat{g}_{mn}\left|\mathcal{H}_1\right.\right\}\\ =&\mathbb{E}\left\{\frac{1}{K}\sum_{k=1}^{K}\left|x_m\left(k\right)\right|^{b/2}\left|x_n^*\left(k\right)\right|^{b/2}\right\}\\ =&\frac{1}{K}\sum_{k=1}^{K}\mathbb{E}\left\{\left|x_m\left(k\right)\right|^{b/2}\left|x_n^*\left(k\right)\right|^{b/2}\right\}\\ \simeq&\mathbb{E}^2\left\{\left|x_m\left(k\right)\right|^{b/2}\right\}\\ =&\mathbb{E}^2\left\{\left|h_m s(k)+w_m\left(k\right)\right|^{b/2}\right\}\\ =&\mathbb{E}^2\left\{\left|w_m(k)\right|^{b/2}+\frac{b}{2}\left|h_m s(k)\right|\left|w_m(k)\right|^{b/2-1}\right.\\ &\left.+\frac{b/2(b/2-1)}{2!}\left|h_m s(k)\right|^2\left|w_m(k)\right|^{b/2-2}+\cdots\right\}.\end{aligned}\tag{59}$$

Assuming GSNR is low, then $|h_m s(k)| \ll |w_m(k)|$, and the higher-order terms of $|h_m s(k)|$ can be ignored. Using $\mathbb{E}\left\{s(k)\right\}=0$ and $\mathbb{D}\left\{s(k)\right\}=\sigma_s^2$, the mean μ_{21} can be rewritten as (60) at the bottom of the page.

Exploiting (60), the second-order moment of $\hat{g}_{mn}$ can be expressed as

$$\begin{aligned}\mathbb{E}\left\{\hat{g}_{mn}^2\left|\mathcal{H}_1\right.\right\}=&\mathbb{E}\left\{\left(\frac{1}{K}\sum_{k=1}^{K}\left|x_m\left(k\right)\right|^{b/2}\left|x_n^*\left(k\right)\right|^{b/2}\right)^2\right\}\\ =&\frac{1}{K^2}\mathbb{E}\left\{\left(\sum_{k=1}^{K}\left|x_m\left(k\right)\right|^{b/2}\left|x_n^*\left(k\right)\right|^{b/2}\right)^2\right\}.\end{aligned}\tag{61}$$

According to $\mathbb{E}\left\{\hat{g}_{mn}\left|\mathcal{H}_1\right.\right\}$ and $\mathbb{E}\left\{\hat{g}_{mn}^2\left|\mathcal{H}_1\right.\right\}$, the variance

$$\begin{aligned}\sigma_{11}^2 =&\mathbb{E}[\hat{g}_{mm}^2|\mathcal{H}_1]-\mathbb{E}^2[\hat{g}_{mm}|\mathcal{H}_1]\\ =&\mathbb{E}\left\{\left(\frac{1}{K}\sum_{k=1}^{K}\left|x_m\left(k\right)\right|^{b/2}\left|x_m^*\left(k\right)\right|^{b/2}\right)^2\right\}-\left(\frac{1}{K}\sum_{k=1}^{K}\mathbb{E}\left\{\left|x_m\left(k\right)\right|^{b/2}\left|x_m^*\left(k\right)\right|^{b/2}\right\}\right)^2\\ =&\frac{1}{K}\left(\mathbb{E}\left\{\left|x_m\left(k\right)\right|^{2b}\right\}-\mathbb{E}^2\left\{\left|x_m\left(k\right)\right|^{b}\right\}\right)\\ \simeq&\frac{1}{K}\left(C(2b,\alpha)\gamma^{2b/\alpha}+b(2b-1)|h_m|^2\sigma_s^2C(2b-2,\alpha)\gamma^{(2b-2)/\alpha}-\mu_{11}^2\right).\end{aligned}\tag{55}$$

$$\begin{aligned}\mu_{21}\simeq&\mathbb{E}\left\{|w_m(k)|^{b/2}+\frac{b/2(b/2-1)}{2!}|h_m s(k)|^2|w_m(k)|^{b/2-2}\right\}\\ =&C(b/2,\alpha)\gamma^{(b/2)/\alpha}+\frac{b/2(b/2-1)}{2}|h_m|^2(\mu_s+\sigma_s^2)C(b/2-2,\alpha)\gamma^{(b/2-2)/\alpha}.\end{aligned}\tag{60}$$

σ_{21}^2 can be obtained as

$$\begin{aligned}\sigma_{21}^2 &= \mathbb{D}\left\{\hat{g}_{mn}\left|\mathcal{H}_1\right.\right\} \\ &= \mathbb{E}\left\{\hat{g}_{mn}^2\left|\mathcal{H}_1\right.\right\} - \mathbb{E}^2\left\{\hat{g}_{mn}\left|\mathcal{H}_1\right.\right\} \\ &= \frac{1}{K}\left(\mathbb{E}\left\{\left|x_m\left(k\right)\right|^{2b}\right\} - \mathbb{E}^4\left\{\left|x_m\left(k\right)\right|^{b/2}\right\}\right) \\ &= \frac{1}{K}\left(\mathbb{E}\left\{\left|x_m\left(k\right)\right|^{2b}\right\} - \left(\mu_{21}\right)^2\right),\end{aligned} \tag{62}$$

where $\mathbb{E}^2\left\{\left|x_m\left(k\right)\right|^b\right\}$ can be approximated as μ_{11}^2, so (62) can be modified as

$$\sigma_{21}^2 \simeq \frac{1}{K}\left(\mu_{11}^2 - \mu_{21}^2\right). \tag{63}$$

REFERENCES

[1] Z. Chu, Z. Zhu, X. Li, F. Zhou, L. Zhen and N. Al-Dhahir, "Resource allocation for IRS-assisted wireless-powered FDMA IoT networks," *IEEE Internet Things J.*, vol. 9, no. 11, pp. 8774-8785, Jun., 2022.

[2] J. Pei, S. Li, Z. Yu, L. Ho, W. Liu and L. Wang, "Federated learning encounters 6G wireless communication in the scenario of internet of things," *IEEE Commun. Standards Mag.*, vol. 7, no. 1, pp. 94-100, Mar. 2023.

[3] M. Liu, Z. Zhang, Y. Chen, J. Ge and N. Zhao, "Adversarial attack and defense on deep learning for air transportation communication jamming," *IEEE Trans. Intell. Transp. Syst.*, early access, Apr. 2023, doi: 10.1109/TITS.2023.3262347.

[4] A. A. Khan, M. H. Rehmani, and A. Rachedi, "Cognitive-radio-based Internet of Things: Applications, architectures, spectrum related functionalities, and future research directions," *IEEE Wireless Commun.*, vol. 24, no. 3, pp. 17-25, Jun. 2017.

[5] L. Zhang and Y.-C. Liang, "Joint spectrum sensing and packet error rate optimization in cognitive IoT," *IEEE Internet Things J.*, vol. 6, no. 5, pp. 7816-7827, Oct. 2019

[6] Y. Chen, Y. Cai, G. Ding, B. Yu and C. Xu, "Age of information for short-packet relay communications in cognitive-radio-based internet of things with outdated channel state information," *IEEE Trans. Cogn. Commun. Netw.*, vol. 9, no. 3, pp. 722-737, Jun. 2023.

[7] J. Adu Ansere, G. Han, H. Wang, C. Choi and C. Wu, "A reliable energy efficient dynamic spectrum sensing for cognitive radio IoT networks," *IEEE Internet Things J.*, vol. 6, no. 4, pp. 6748-6759, Aug. 2019.

[8] A. Gharib, W. Ejaz and M. Ibnkahla, "Distributed spectrum sensing for IoT networks: architecture, challenges, and learning," *IEEE Internet of Things Mag.*, vol. 4, no. 2, pp. 66-73, Jun. 2021.

[9] X. Liu, K. Zheng, K. Chi and Y. H. Zhu, "Cooperative spectrum sensing optimization in energy-harvesting cognitive radio networks," *IEEE Trans. Wireless Communi.*, vol. 19, no. 11, pp. 7663-7676, Nov. 2020.

[10] F. F. Digham, M.-S. Alouini, and M. K. Simon, "On the energy detection of unknown signals over fading channels," *IEEE Trans. Commun.*, vol. 55, no. 1, pp. 21-24, Jan. 2007.

[11] Y. Zeng and Y. C. Liang, "Eigenvalue-based spectrum sensing algorithms for cognitive radio," *IEEE Trans. Commun.*, vol. 57, no. 6, pp. 1784-1793, Jun. 2009.

[12] A. Mariani, A. Giorgetti, and M. Chiani, "Effects of noise power estimation on energy detection for cognitive radio applications," *IEEE Trans. Commun.*, vol. 59, no. 12, pp. 3410-3420, Dec. 2011.

[13] X. Zhang, R. Chai, and F. Gao, "Matched filter based spectrum sensing and power level detection for cognitive radio network," in *Proc. IEEE Glob. Conf. Signal Inf. Process. (GlobalSIP)*, 2014, pp. 1267-1270.

[14] S. Dikmese, P. C. Sofotasios, M. Renfors, and M. Valkama, "Subband energy based reduced complexity spectrum sensing under noise uncertainty and frequency-selective spectral characteristics," *IEEE Trans. Signal Process.*, vol. 64, no. 1, pp. 131-145, Jan. 2016.

[15] A. Chaturvedi, K. Prasad, S. K. Jha, V. Srinivas, N. Anil Kumar and V. Dankan Gowda, "Approaches for advanced spectrum sensing in cognitive radio networks," in *Proc. Int. Conf. Intell. Comput. Control Syst. (ICICCS)*, 2023, pp. 1485-1490.

[16] R. Senanayake, P. J. Smith, P. A. Dmochowski, A. Giorgetti, and J. S. Evans, "Mixture detectors for improved spectrum sensing," *IEEE Trans. Wireless Commun.*, vol. 19, no. 6, pp. 4335-4348, Jun. 2020.

[17] X. Tong, Y. Hu, Z. Shen, C. Shen and Y. Li, "A novel multi-antenna iterative spectrum sensing algorithm based on the SUMPLE scheme," in *Proc. IEEE Int. Symposium Broadband Multimedia Syst. Broadcast.*, 2016, pp. 1-6.

[18] Y. Zeng and Y. C. Liang, "Maximum-minimum eigenvalue detection for cognitive radio," in *Proc. IEEE Int. Symp. Pers. Indoor Mobile Radio Commun.*, 2007, pp. 1-5.

[19] Q. Jia, B. Li, S. Ma and M. Liu, "Local variance detection for multi-antenna spectrum sensing," *IEEE Commun. Lett.*, vol. 19, no. 12, pp. 2142-2145, Dec. 2015.

[20] M. Lin, W. Wang, X. Hong, and W. Zhang, "GLRT approach for multiantenna-based spectrum sensing under interference," *IEEE Commun. Lett.*, vol. 24, no. 7, pp. 1524-1528, Jul. 2020.

[21] A. Z. Chen and Z. P. Shi, "A real-valued weighted covariance-based detection method for cognitive radio networks with correlated multiple antennas," *IEEE Commun. Lett.*, vol. 22, no. 11, pp. 2290-2293, Nov. 2018

[22] P. Urriza, E. Rebeiz, and D. Cabric, "Multiple antenna cyclostationary spectrum sensing based on the cyclic correlation significance test," *IEEE J. Sel. Areas Commun.*, vol. 31, no. 11, pp. 2185-2195, Nov. 2013.

[23] T. M. Getu, W. Ajib, and R. Landry, "Simple F-test-based spectrum sensing techniques for multi-antenna cognitive radios," *IEEE Trans. Commun.*, vol. 66, no. 11, pp. 5081-5096, Nov. 2018

[24] K. Chae and Y. Kim, "DS2MA: A deep learning-based spectrum sensing scheme for a multi-antenna receiver" *IEEE Wireless Commun. Lett.*, vol. 12, no. 6, pp. 952-956, Jun. 2023.

[25] J. Li, D. Z. Feng and W. X. Zheng, "A robust decision directed algorithm for blind equalization under α-stable noise," *IEEE Trans. Signal Process.*, vol. 69, pp. 4949-4960, July 2021.

[26] X. Yan, G. Liu, H.-C. Wu, G. Zhang, Q. Wang, and Y. Wu, "Robust modulation classification over α-stable noise using graph-based fractional lower-order cyclic spectrum analysis,"*IEEE Trans. Veh. Technol.*, vol. 69, no. 3, pp. 2836-2849, Mar. 2020.

[27] Tsung-Hsien Liu and J. M. Mendel, "A subspace-based direction finding algorithm using fractional lower order statistics," *IEEE Trans. Signal Process.*, vol. 49, no. 8, pp. 1605-1613, Aug. 2001.

[28] J. Park, G. Shevlyakov, and K. Kim, "Maximin distributed detection in the presence of impulsive alpha-stable noise," *IEEE Trans. Wireless Commun.*, vol. 10, no. 6, pp. 1687-1691, Jun. 2011.

[29] Zhu, Xiaomei , W. P. Zhu , and B. Champagne, "Spectrum sensing based on fractional lower order moments for cognitive radios in alpha-stable distributed noise," *Signal Process.* 111, pp. 94-105, 2015.

[30] Z. Shabani and A. M. A. Modarres, "A new nonlinear technique for spectrum sensing in the presence of impulsive noise," in *Proc. 22nd Iranian Conf. Electrical Engineering*, 2014, pp. 1605-1609.

[31] K. Hassan, R. Gautier, I. Dayoub, M. Berbineau and E. Radoi, "Multiple-antenna-based blind spectrum sensing in the presence of impulsive noise," *IEEE Trans. Veh. Technol.*, vol. 63, no. 5, pp. 2248-2257, Jun 2014.

[32] S. Gurugopinath and R. Muralishankar, "Geometric power detector for spectrum sensing under symmetric alpha stable noise," *Electronics Letters*, vol. 54, no. 22, pp. 1284-1286, Nov. 2018.

[33] M. Liu, N. Zhao, J. Li and V. C. M. Leung, "Spectrum sensing based on maximum generalized correntropy under symmetric alpha stable noise," *IEEE Trans. Veh. Technol.*, vol. 68, no. 10, pp. 10262-10266, Oct. 2019.

[34] H. Qu, X. Xu, J. Zhao, F. Yan, and W. Wang, "Robust spectrum sensing based on hyperbolic tangent in Gaussian and non-Gaussian noise environments," in *Proc. 10th Int. Conf. Ubiquitous Future Netw.*, 2018, pp. 283-288.

[35] H. Qu, X. Xu, J. Zhao, F. Yan, and W. Wang, "A robust hyperbolic tangent-based energy detector with Gaussian and non-Gaussian noise environments in cognitive radio system," *IEEE Syst. J.*, vol. 14, no. 3, pp. 3161-3172, Sep. 2020.

[36] A. Mehrabian, M. Sabbaghian, and H. Yanikomeroglu, "Spectrum sensing for symmetric α-stable noise model with convolutional neural networks," *IEEE Trans. Commun.*, vol. 69, no. 8, pp. 5121-5135, Aug. 2021.

[37] J. Morales, A. Flores Riveros, "The generalization of the binomial theorem," *J. Math. Phys.* 30, pp. 393-397, 1989.